

## Reaction Dynamics of $\text{NH}_2+\text{OH}$ on an Interpolated Potential Energy Surface

S.H. Mousavipour\*, F. Pirhadi and S. Ramazani<sup>†</sup>

*Department of Chemistry, College of Science, Shiraz University, Shiraz, 71454, Iran*

*<sup>†</sup>Department of Chemistry, Yasouj University, Yasouj, Iran*

*(Received 17 February 2013, Accepted 30 November 2013)*

A potential energy surface, describing the behavior of the title reaction, has been constructed by interpolation of *ab initio* data.  $\text{H}_2\text{O}$ ,  $\text{NH}$ ,  $\text{HON}$ ,  $\text{HNO}$ ,  $\text{NH}_3$ ,  $\text{O}$ ,  $\text{H}_2\text{NO}$ , *cis* or *trans*- $\text{HONH}$ ,  $\text{H}$  products, two vibrationally energized  $\text{NH}_2\text{OH}^*$  and  $\text{NH}_3\text{O}^*$  adducts were observed. The reaction probabilities, effective cross sections, and branching ratios for different channels are reported. The rate constant for the formation of the  $\text{NH}_2\text{OH}^*$  is calculated as a function of effective cross section and is compared with the available data in the literature. The calculated QCT rate constant for the formation of  $\text{NH}_2\text{OH}$  was found to be lower than that reported in our previous study (*J. Phys. Chem. A*, **113**, 12961, 2009) based on the RRKM method with steady state assumption for the formation of energized adducts that could be due to the lack of the stabilization process in QCT calculations.

**Keywords:** Reaction dynamics, Amidogen radical, Hydroxyl radical, Effective cross section

## INTRODUCTION

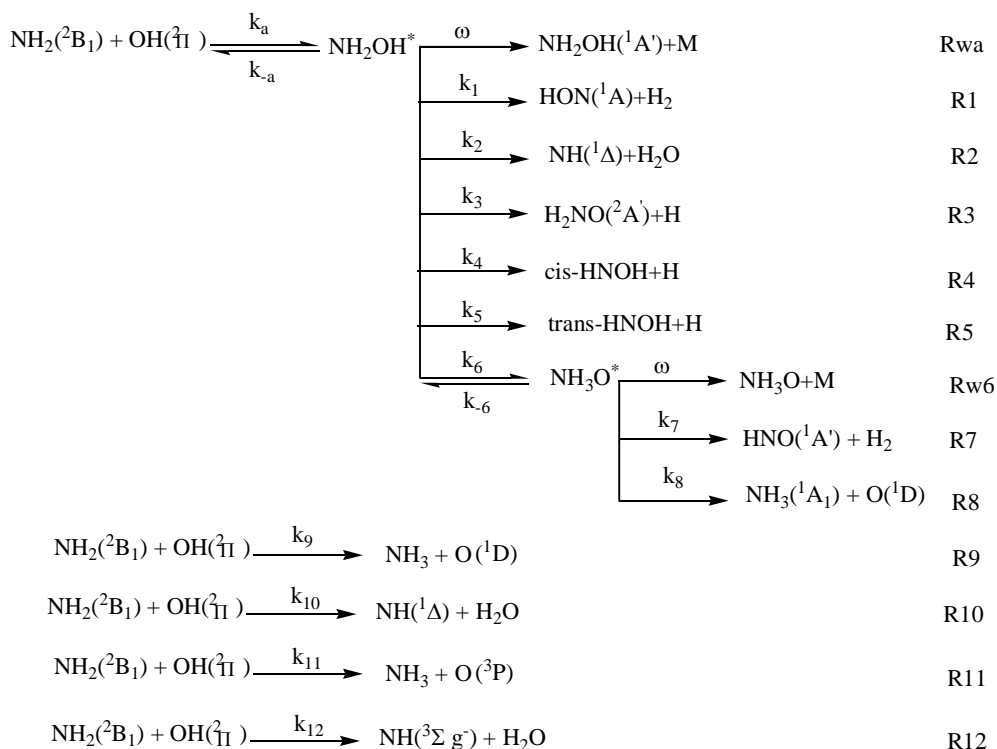
Amidogen,  $\text{NH}_2$ , and hydroxyl radicals are two important reactive species in the atmospheric processes and combustion chemistry. The reactions of amidogen radical with the other reactive species are important for understanding the thermal dissociation of  $\text{NO}_x$  process [1], in which  $\text{NO}$  that is formed during combustion is converted into the molecular nitrogen. One of the reactions in this system,  $\text{NH}_2 + \text{OH} \rightarrow \text{NH} + \text{H}_2\text{O}$ , is considered to be a kinetically sensitive reaction in the thermal dissociation of  $\text{NO}_x$  process [2] and in the gas-phase oxidation of ammonia [3]. The reactions of  $\text{NH}_x$  species with  $\text{H}_2\text{O}$  species have been investigated by several experimental and theoretical studies, and have been reviewed to some extent [4]. The kinetics of the reaction of  $\text{NH}_2 + \text{OH}$  has been studied by different groups [5-25]. In 2009, we reported a detailed mechanism and kinetics of the title reaction to reveal its complexity [24]. On the basis of the available data in the literature and our *ab initio* calculations, we proposed a possible mechanism for the title reaction on both lowest

singlet and triplet surfaces, Ref. [24], shown in Scheme 1. A schematic of the potential energy diagram on the lowest singlet surface at the CCSD(full)/Aug-cc-pVTZ level is shown in Fig. 1.

As shown in Scheme 1, the complexity of this system is relatively high and formation of energized  $\text{NH}_2\text{OH}^*$  has a prominent role on this complexity. No barrier height was found for the association of the reactants in the title reaction to form this chemically activated molecule that is capable of rearrangement or dissociation processes or recrossing back to the reactants at lower pressures.

The detail of the proposed mechanism in Scheme 1 has been discussed in Ref. [24], therefore we would not reemphasize on those aspects here. There are two deep potential energy wells (formation of energized  $\text{NH}_2\text{OH}^*$  and  $\text{NH}_3\text{O}^*$ ) on the singlet surface of the title reaction that play important role in the kinetics of this system. The reason for the need of more elucidation of the kinetics of this system is the complexity caused by those deep wells in this system. The first step of the title reaction is association of the reactants, reaction  $R_{wa}$ , to produce hydroxylamine. The produced energized hydroxylamine could be very floppy at energies above the barriers to do *cis-trans* isomerization or

\*Corresponding author. E-mail: mousavi@susc.ac.ir



Scheme 1

formation of ammonia oxide ( $\text{NH}_3\text{O}$ ) beside the other dissociative paths shown in Fig. 1. It has been suggested the O-H stretching vibration in  $\text{NH}_2\text{OH}$  could couple to the other vibrational modes in this molecule particularly well [25]. It would be interesting to explore dynamics behavior of such systems where a barrier-less association reaction causes the formation of a chemically activated adduct that is placed in a potential well. How this activated species behaves while an excess amount of the energy is confined within one of its internal degrees of freedom. Scott *et al.* [25] have experimentally studied the IVR behavior of vibrationally excited hydroxylamine. To the best of our knowledge, no dynamical study on the title reaction has been reported yet. This is the purpose of the present study to investigate the dynamics of the title reaction on its first singlet potential energy surface, as shown in Fig. 1. Dynamics calculations make it possible to assess the proposed reaction mechanism more clearly, view the transition states behavior (where chemical bonds are broken or formed), and examine the possible presence of resonances in the deep potential intermediates. Dynamical

calculations enable one to obtain reaction probabilities and cross sections for the fundamental channels and to simulate strongly nonequilibrium flows.

To simulate the dynamics of a reaction, its potential energy surfaces (PESs) need to be known for a large number of molecular configurations [26]. Quantum chemical methods [27], either prior to the dynamics simulation or “on-the-fly” [28] during the dynamics can be used to study the dynamics of a reaction. However, as the computational cost of *ab initio* calculations rises steeply with the demand for accuracy, and with the number of electrons, compromises are usually made between the cost and the quality of the PES and hence most dynamics simulations are based on approximated PESs [29].

Collins introduced and developed a method named Growing Potential Energy Surfaces to construct molecular PES with classical trajectory simulations to provide an iterative scheme for successively improving the surface [30]. The GROW methodology does not assume a functional form for the PES. According to this interpolation scheme, the energy at an arbitrary geometry is expressed as

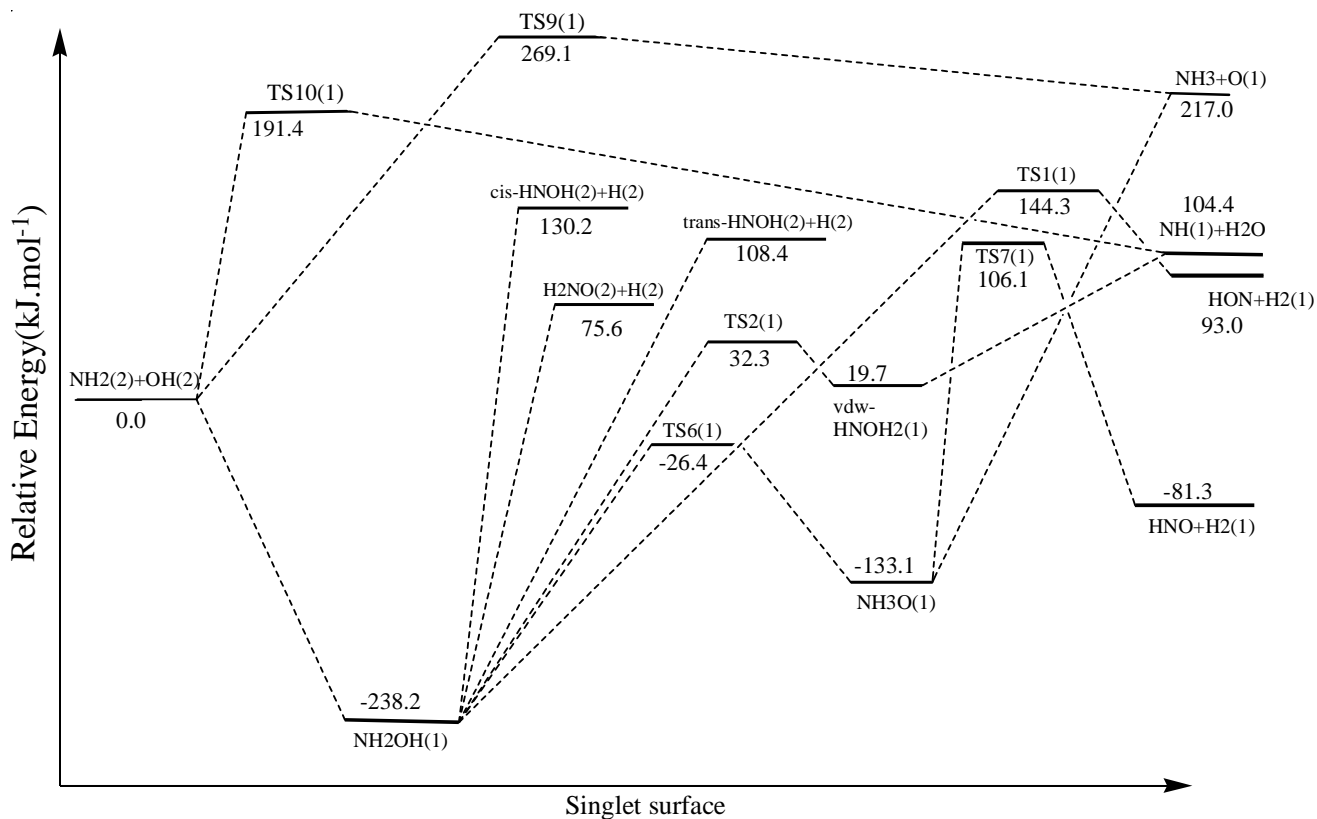


**Fig. 1.** Relative energies of the stationary points in  $\text{kJ mol}^{-1}$  on the lowest singlet surface at the CCSD (full)/Aug-cc-pVTZ level. All values are corrected for zero-point energies.

a weighted sum of Taylor series expansions from neighboring data points, where the required energy and derivative data are obtained from *ab initio* calculations. The method requires the energy, gradient, and second derivative of the potential with respect to internal coordinates at important sampled locations on the PES. The iterative procedure automatically places new data points only in regions of configuration space that are important dynamically, so that the PES may be accurately determined using surprisingly few calculations [30]. This minimizes the number of data points required to accurately characterize the surface, thus enabling correspondingly higher level calculations to be performed [30,31]. The data on the potential energy surface are obtained from *ab initio* calculations. An interpolation and/or extrapolation are/is then made from the existing data points to any location on the PES. It is important to realize that the method is fully

automated and does not require any least-square fitting. Collins' PES construction method has recently been successfully combined with *ab initio* calculations and quantum reactive scattering code or using classical trajectories rather than quantum reactive scattering and has been applied to numerous reactions [31]. The details of the Grow methodology have been presented previously [30-32], so only a brief description is given here.

For systems with more than four atoms, a set of  $3N-6$  algebraically independent linear combinations of the  $N(N-1)/2$  reciprocal bond lengths, can be constructed automatically at each geometry  $\mathbf{Z}(i)$  [33]. In general, a surface is constructed by expanding the surface in the vicinity of a "data point" as a Taylor series in the inverse distances,  $\mathbf{Z}$ , where  $Z_k = 1/R_k$  and  $\mathbf{R}$  is the set of interatomic distances. More physically reasonable behavior is obtained when the Taylor expansion is written in terms of inverse

distances  $\mathbf{Z}$  rather than interatomic distances,

$$T_i(\mathbf{Z}) = V[\mathbf{Z}(i)] + \sum_{k=1}^{3N-6} [Z_k - Z_k(i)] \frac{\partial V}{\partial Z_k} \Big|_{\mathbf{Z}=\mathbf{Z}(i)} + \frac{1}{2!} \sum_{k=1}^{3N-6} \sum_{j=1}^{3N-6} [Z_k - Z_k(i)][Z_j - Z_j(i)] \times \frac{\partial^2 V}{\partial Z_k \partial Z_j} \Big|_{\mathbf{Z}=\mathbf{Z}(i)} + \dots \quad (1)$$

where  $V[\mathbf{Z}(i)]$  is the potential energy at  $\mathbf{Z}(i)$  and derivatives are taken with respect to inverse distances at the  $i$ th data point  $\mathbf{Z}(i)$ . The expansion is truncated to second order.

For a system with more than four atoms, redundant internal coordinates can occur since the number of inter-nuclear distances is greater than the number of independent internal coordinates,  $3N-6$ . In general, the interpolation coordinates are an over-complete set of curvilinear coordinates. In this case, a set of  $3N-6$  local internal coordinates  $\xi$  are constructed as linear combinations of the  $N(N-1)/2$  reciprocal distances for each  $\mathbf{Z}(i)$  [33],

$$\xi^{(X_0)}(X) = \bar{U}^T Z \quad \text{for } Z \text{ close to } Z_0 = Z(X_0) \quad (2)$$

where  $X_0$  refers to the initial set of Cartesian coordinates. The matrix  $\mathbf{U}$  is defined in terms of molecular fragments, using both intra- and intermolecular distances. The QM Cartesian derivatives of the PES at  $X(i)$  must then be transformed into these internal coordinates. The Taylor series in Eq. (1) is then evaluated using these internal coordinates in place of the reciprocal distances.

Once the required QM energy and derivatives were evaluated at some number ( $N_d$ ) of molecular configurations, a modified Shepard interpolation [34] defines the total potential energy  $V(\mathbf{Z})$  at any configuration  $\mathbf{Z}$  as a weighted average of Taylor series about all  $N_d$  initial data points and their symmetry-determined equivalents,

$$V(\mathbf{Z}) = \sum_{g \in G} \sum_{i=1}^{N_{data}} w_{g^o i}(\mathbf{Z}) T_{g^o i}(\mathbf{Z}) \quad (3)$$

where, the sum over  $i$  iterates over the  $N_{data}$  geometries (data points) at which *ab initio* calculations have been performed to evaluate the potential energy and its first and second

derivatives. The  $T$ s are second order Taylor series expansions for the energy around each data point. The quantity  $w$  is a normalized weight function that is constructed to ensure an interpolation of the *ab initio* data. The subscript " $g^o i$ " denotes that the quantity is for permutation  $g$  of data point  $i$ .  $G$  is the symmetry group of the molecule, generally the complete nuclear permutation group. Thus, the sum over  $G$  means that all permutationally equivalent geometries are included in the expansion, so the interpolated potential obeys the underlying permutation symmetry.

The normalized weight function  $w_i$  weights the contribution of a Taylor expansion at  $\mathbf{Z}(i)$  to the total PE at configuration  $\mathbf{Z}$ ,

$$w_i = \frac{v_i(\mathbf{Z})}{\sum_{g \in G} \sum_{k=1}^{N_d} v_{g^o k}(\mathbf{Z})} \quad (4)$$

Data points that are spatially close to  $\mathbf{Z}$  will have a larger weight. The biasing of data is achieved using the unnormalized two-part weight function  $v_i(\mathbf{Z})$ ,

$$v_i(\mathbf{Z}) = \frac{1}{\left[ \sum_{l=1}^{N(N-1)/2} \left( \frac{Z_l - Z_l(i)}{d_l(i)} \right)^{2q} \right]^q + \left[ \sum_{l=1}^{N(N-1)/2} \left( \frac{Z_l - Z_l(i)}{d_l(i)} \right)^{2p} \right]^p} \quad \text{for } q \ll p \quad (5)$$

Here  $q = 2$  and  $2p \gg 3N-3$  [35], and the  $\{d_l(i)\}$  effectively define a type of confidence volume about  $\mathbf{Z}(i)$ . If the components of  $\mathbf{Z}$  fall within the "confidence lengths" of  $\mathbf{Z}(i)$ , the weight assigned to  $\mathbf{Z}(i)$  will fall slowly as the effective distance,  $\|\mathbf{Z}-\mathbf{Z}(i)\|$ , increases. If  $\mathbf{Z}$  falls outside the confidence length, the weight assigned to  $\mathbf{Z}(i)$  falls quickly with an increase in distance. The confidence lengths are determined through a Bayesian analysis [36]. This two-part weight function allows the relative weights of two or more data points near  $\mathbf{Z}$  to vary only slowly with varying  $\mathbf{Z}$ ; this reduces the error in the PES gradient and is especially important for larger systems [30].

The basic iterative procedure is as follows [37]. After constructing a small initial data set, usually on a relevant reaction path (the Shepard interpolation is thus well defined

on this reaction path), GROW runs a small number of trajectories with initial conditions appropriate to the reaction under study. Molecular configurations are periodically recorded to obtain a set of several thousands of geometries. One or more of these geometries is chosen to be added to the data set, and the required QM energies and derivatives are calculated for these points. Finally, the new data points are incorporated into the data set to form an updated PES. This process continues with the calculation of more trajectories. As the data set grows, the interpolated PES becomes more accurate. The PES is considered to be converged to chemical accuracy when the average values of observables of interest (obtained from large sets of classical trajectories) are unchanged by further iterations and increase in the size of the data set.

The methods for choosing a new data point in GROW have been described in detail by Thompson and Collins in Ref. [32]. The variance sampling method attempts to place data points at configurations where the uncertainty in the interpolated PE is the highest. The “*h*-weight” method [38] attempts to place data in regions that the trajectories often visit, but where few data points are already present. Both methods are used alternately to give a more “well-rounded” description of the PES.

This work elucidates new atomic-level mechanistic information that may be common in a range of chemical reactions, and our findings are important for the understanding of the nature of the dynamics of polyatomic interactions and behavior of a chemically activated molecule in a deep well. A global 9-dimensional *ab initio* potential energy surface (PES), describing the interaction of OH radical with NH<sub>2</sub> radical, is constructed based on the modified Shepard interpolation method [30,34]. These dynamical calculations on our proposed PES reveal interesting features of detailed dynamical quantities.

### Constructing the PES

The study of reactive or nonreactive chemical processes on a molecular level requires a well knowledge of the PES for the system under consideration. The nature of the PES can be probed either experimentally or by using *ab initio* quantum chemical calculations.

In this study, the PES has been computed as a modified Shepard interpolation over a data set of *ab initio* points

using the Grow methodology.

Gaussian03 program was used to optimize and calculate the energies of the stationary points at the MPWb1K and MP2 levels of theory. The derivatives were calculated at the MP2/6-311+G(d,p) level. Ninety five data points from *ab initio* calculations along the reaction coordinate were used as the starting points to describe the whole regions of the PES for the title reaction. The Grow program used this initial data set to run a small number of trajectories with initial conditions appropriate to the title reaction that will be discussed later in this section. In growing the PES process by the Grow program, molecular configurations are periodically recorded to obtain a set of several thousands of geometries. One or more of these geometries is chosen to be added to the data set after each iteration, and the Grow program calculated the required QM energies and derivatives for these points. Finally, the new data points are incorporated into the set of the initial data points to form an updated PES. The program automatically carried out the variance sampling method and “*h*-weight” method (as discussed in Ref. [30]) alternately to choose a new data point to construct a more “well-rounded” PES. This process continues with the calculation of more trajectories to grow the data set, resulting in more accurate interpolated PES. The process was iterated until the calculated reaction probability or effective cross section was supposed to be sufficiently converged, indicating that dynamically relevant regions of the interpolated PES were determined accurately. Whereupon the grow procedure for the NH<sub>2</sub> + OH reaction was continued, 2000 data points describing various channels of the reaction from classical trajectory calculations were added to the initial data set.

The initial states for the trajectories were selected from the irrotational microcanonical ensemble for each fragment at the energy corresponding to the correct zero point energy, taken as 47.8 and 21.3 kJ mol<sup>-1</sup> for NH<sub>2</sub> and OH, respectively. The initial center of mass separation was set to 10.0 Å, a value considered sufficiently large to make the interaction energy essentially negligible, and the impact parameter selected from a linear distribution of the  $N(N-1)/2$  reciprocal bond lengths with a maximum impact parameter of up to 9.0 Å (depending on the relative translational energy).

The maximum value of the impact parameter,  $b_{\max}$ , was

determined at each translational energy in the range of  $E_t = 25.2$ - $157.5$  kJ mol<sup>-1</sup> by computing batches of 600 trajectories at fixed values of  $b$ , systematically increasing the size of  $b$  until no reaction was observed in the batch of 600 trajectories. The reactive cross section at each translational energy is defined as;

$$\sigma(E_t) = \pi (b_{max})^2 P_r \quad (6)$$

where  $P_r$  is the ratio of the number of reactive trajectories,  $N_r$ , to the total number of trajectories,  $N_T$ . A FORTRAN program was used to select those structures that their geometries were close to one of the reactant, intermediate, or product geometries to calculate the  $P_r$  for each product.

A standard velocity-Verlet integrator was used to calculate the classical equations of motion for the atoms with a time step of 0.01fs. A Markov walk was used to generate a microcanonical distribution of initial atomic positions and velocities for the classical trajectories. The number of Markov chain steps per trajectory and Markov step length were set at 500 and 0.15 Å, respectively, for all fragments. To grow the PES, no saddle point geometry was used as the initial reference geometry.

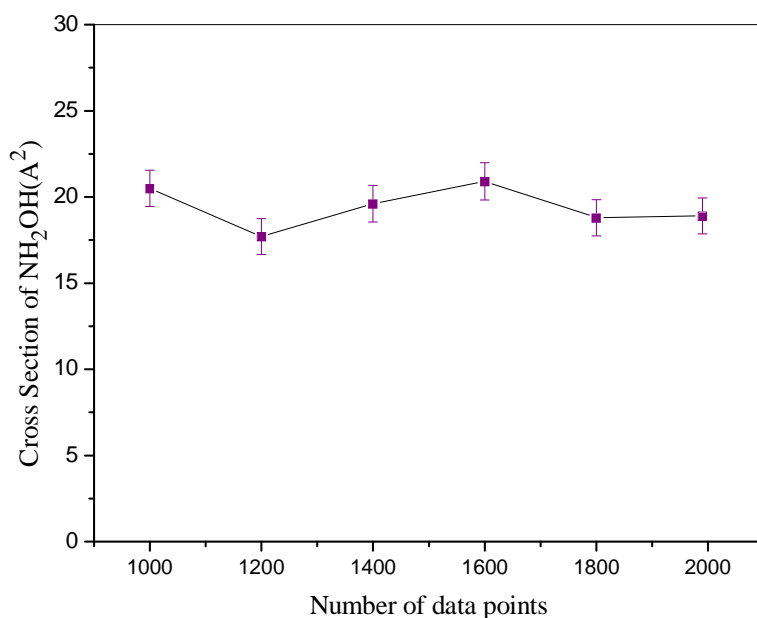
### General Features of the PES and Results

To ensure that adding the number of data points to the *ab initio* data set does not alter the dynamical quantities, the effect of increasing the data set size was tested on the calculated effective cross section. Figure 2 shows the convergence of the reaction cross section as a function of PES data set size calculated from batches of 2000 trajectories at an initial relative translational energy of 25.2 kJ mol<sup>-1</sup> for the formation of NH<sub>2</sub>OH. The error bars indicate one standard error either side of the calculated value. This figure shows that adding the final several hundred data points, out of the total of 2000 data points, does not significantly alter the calculated cross section. These results are typical of calculations at higher translational energies. Figure 3 shows the effect of increasing the impact parameter on the probability of formation of the energized NH<sub>2</sub>OH\* as a function of relative kinetic energy. We have shown in Fig. 3 that reaction probability for the formation of NH<sub>2</sub>OH decreases by increasing the relative kinetic energy, as expected for

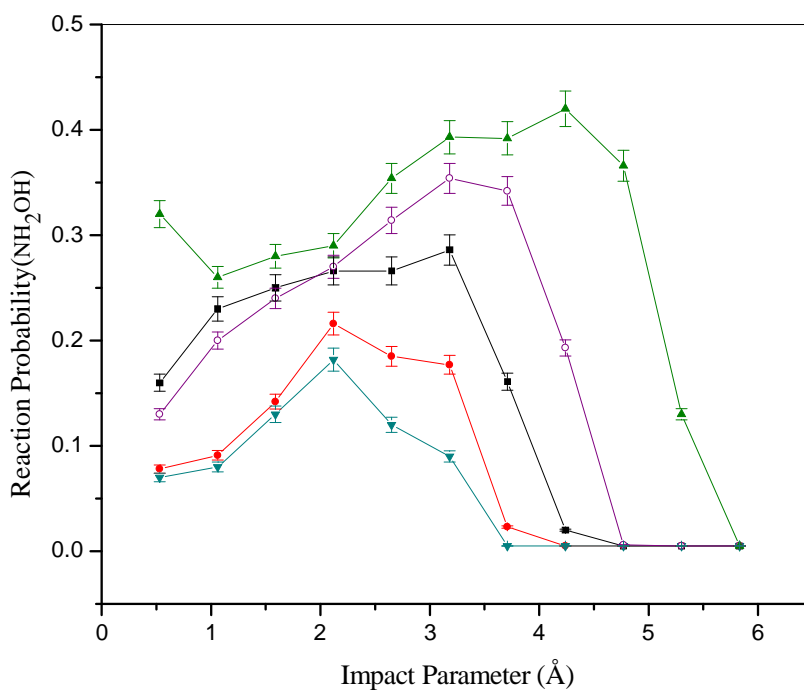
barrierless association reactions. Figure 4 shows the variation of the effective cross sections for the formation of various products of this system as a function of relative translational energy. As shown, the pattern of changing the cross sections for different channels depends on the nature of each path, which two different issues should be taken under consideration. One aspect is to consider the absolute values of the effective cross sections for different paths. As shown in Figs. 4a to 4h, the formation of NH<sub>2</sub>OH\* has the maximum cross section and formation of HNOH + H and NH + H<sub>2</sub>O have the next largest effective cross sections relative to the other paths. Another aspect is the position of the maximum of effective cross section relative to the kinetic energy for each individual channel. As expected for association reactions like reaction Rwa,  $b_{max}$  is found to decrease with increasing translational energy, Fig. 4a. According to suggested mechanism for this system, at least two different paths produce NH + H<sub>2</sub>O, reactions R2 and R10. The effective cross section for the formation of NH + H<sub>2</sub>O, as shown in Fig. 4b, has a maximum value at  $81.5 \pm 10.0$  kJ mol<sup>-1</sup> of relative kinetic energy. The same trend is observed for the other channels in Fig. 4. Two features control the value of the effective cross section for different channels; one is the internal energy flow from newly formed N-O bond in the chemically activated NH<sub>2</sub>OH\* to the other internal modes, IVR process, and the other one is the amount of available relative kinetic energy that make the total energy necessary to surmount the corresponding barrier height for each path.

Figure 5 shows the branching ratio for the formation of various products from the energized NH<sub>2</sub>OH\* over the translational energy range of 25.2 kJ mol<sup>-1</sup> to 157.5 kJ mol<sup>-1</sup>. As shown in Fig. 5, the major products at higher translational energies are NH + H<sub>2</sub>O, while at moderate translational energies (about 80 kJ mol<sup>-1</sup>) *cis* or *trans*-HNOH is the major path.

Table 1 summarizes the results of trajectory calculations as a function of relative translational energy. In Table 1, the non-converged trajectories removed from the total number of runs,  $N_T$ .  $N_C$  and  $N_r$  are the number of NH<sub>2</sub>OH complex forming trajectories and the number of trajectories ending to one of the products in this system, respectively.  $N_{rec}$  is the number of recrossing trajectories (those trajectories that form NH<sub>2</sub>OH\* complex but subsequently re-dissociate back



**Fig. 2.** Calculated cross sections for the formation of  $\text{NH}_2\text{OH}^*$  as a function of the PES data set size. The error bars denote plus and minus one standard deviation expected for 2000 trajectories. The connecting lines are merely visual aids.



**Fig. 3.** Reaction probabilities are shown as a function of impact parameter for  $\text{NH}_2+\text{OH}$  collision at relative kinetic energies of ( $\blacktriangle$ ) 25.2  $\text{kJ mol}^{-1}$ , ( $\circ$ ) 81  $\text{kJ mol}^{-1}$ , ( $\blacksquare$ ) 105  $\text{kJ mol}^{-1}$ , ( $\bullet$ ) 131.3  $\text{kJ mol}^{-1}$ , ( $\blacktriangledown$ ) 157.5  $\text{kJ mol}^{-1}$ . The lines are just to follow the symbols.

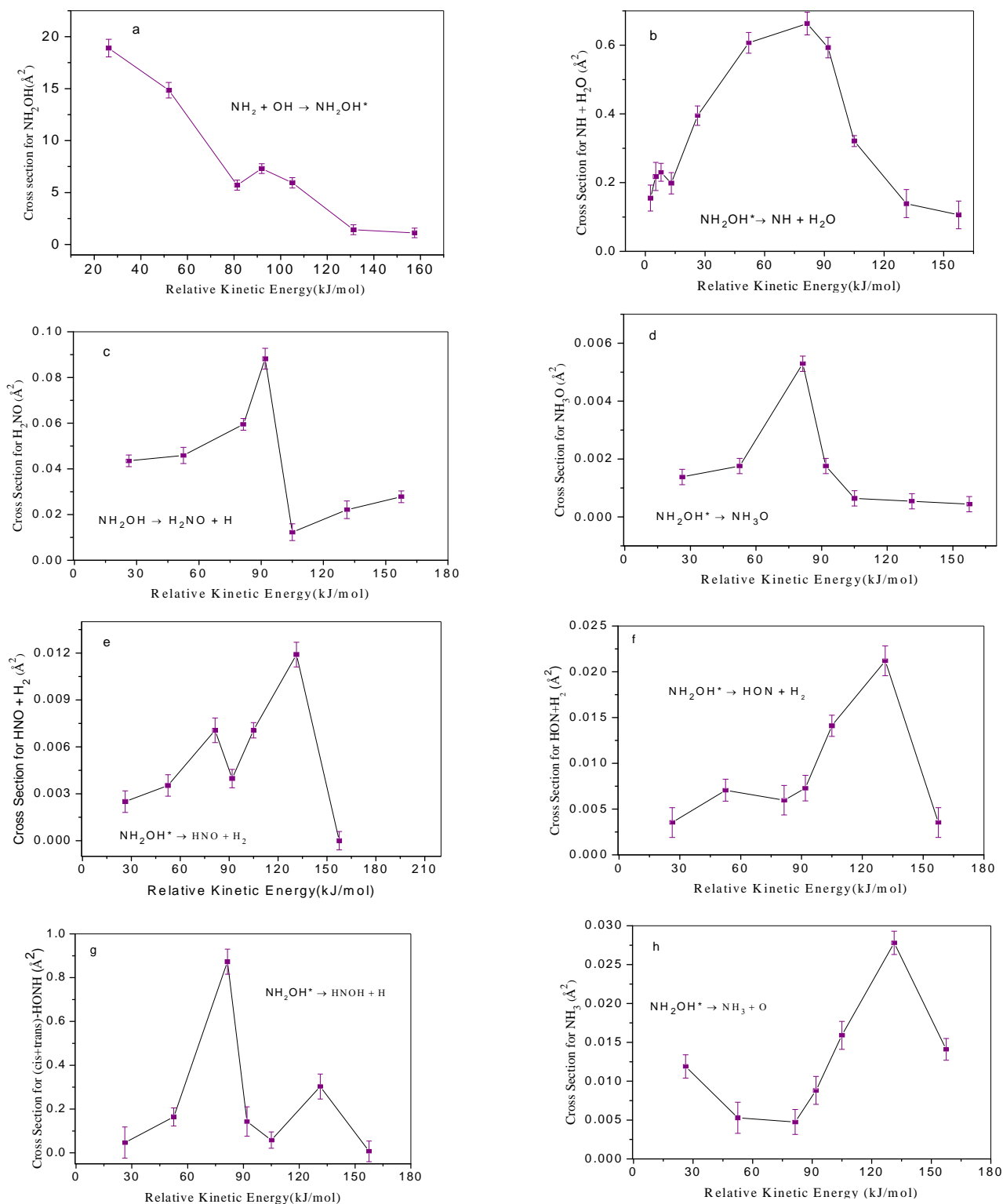


**Fig. 4.** Calculated effective cross sections as a function of relative kinetic energy for the formation of (a)  $\text{NH}_2\text{OH}$ , (b)  $\text{NH} + \text{H}_2\text{O}$ , (c)  $\text{H}_2\text{NO} + \text{H}$ , (d)  $\text{NH}_3\text{O}$ , (e)  $\text{HNO} + \text{H}_2$ , (f)  $\text{HON} + \text{H}_2$ , (g) (*cis* or *trans*)  $\text{HONH} + \text{H}$ , and (h)  $\text{NH}_3 + \text{O}$  formation for 2000 trajectory.

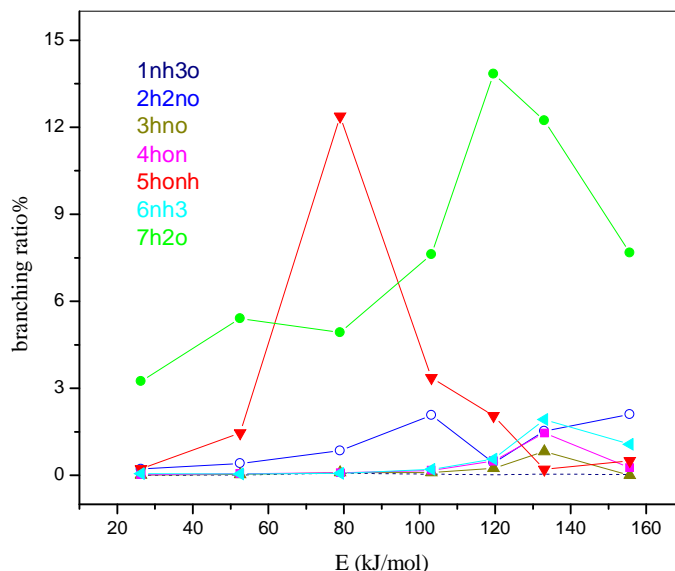


**Fig. 5.** Branching ratios for different channels. (●) for  $\text{H}_2\text{O}$  formation, (▼) for  $\text{HNOH}$  (*cis* & *trans*) formation, (O) for  $\text{H}_2\text{NO}$  formation, (◄) for  $\text{NH}_3$  formation, (■) for  $\text{HON}$  formation, (---) for  $\text{NH}_3\text{O}$  formation.

**Table 1.** Summary of the Trajectory Calculations at Different Relative Kinetic Energies

$E_{tr}$ (kJ mol <sup>-1</sup> )	$b_{max}$ (Å)	$P_r$	$\sigma(E_{tr})$ (Å <sup>2</sup> )	$N_T$	$N_C$	$N_{rec}$	$N_r$
2.5	8.5	0.89	202.0	1691	1580	75	1505
4.6	6.7	0.84	118.0	1561	1440	127	1311
10.5	4.8	0.71	51.3	1560	1334	226	1108
26.3	4.2	0.35	18.9	1751	1188	575	613
52.3	3.6	0.26	10.4	1840	1415	937	478
81.2	3.1	0.19	5.7	1901	1507	1146	361
92.0	2.6	0.18	3.8	1894	1576	1235	341
105.0	2.1	0.18	2.5	1670	1542	1241	301
131.4	2.1	0.08	1.1	1801	1457	1303	154

to the reactants). The reaction probability,  $P_r$ , is defined as the ratio of  $N_r$  to  $N_T$ .

Some of the trajectories are unacceptable in a nonclassical world. The reason is the transfer of a large amount of the vibrational energy to the translational energy

that is a consequence of the fact that in a classical world the energy has no lower bound. Thus, in a classical world, a large amount of vibrational energy accumulated in  $\text{NH}_2\text{OH}^*$  is transferred to the translational energy of the reactants in case of recrossing process or to the translational energy of

the products in case of dissociative or rearrangement processes, where the vibrational energies of these species can lay below their vibrational zero point energies (ZPE). These reactive or recrossing trajectories need to be removed from our calculations, since they are an artifact of the QCT calculations and are not allowed in the quantized real world. Many strategies have been proposed to correct the problem (see, for instance, Ref. [39] and references therein). Here, we employed a so-called passive method [21] and discarded all those reactive trajectories with ZPE-leakage. Here, we have to emphasize that for the ZPE-leakage problem, normally the calculated rate constants from QCT are over estimated.

Once the  $\text{NH}_2\text{OH}$  is formed, the vibrational energy of OH is transferred to the other modes. Thus, when the trajectory dissociates back to the reactants, it often does so by losing the vibrational energy with respect to its original value, in this case the ground-state vibrational energy. In fact, only for high translational energies, does OH keep its vibrational energy above ZPE. As a result, nearly all recrossing trajectories in the low-translational energy regime suffer from ZPE-leakage. Disregarding such trajectories from the final statistics may imply that reactivity will likely be overestimated with respect to the traditional QCT value as the statistics of the reactive trajectories gets improved with respect to the non-reactive one [40].

As the results, only those trajectories for which the total vibrational energy of the products exceeds the sum of their corresponding ZPEs are included in the statistical analysis. The QCT results obtained after discarding these reactive trajectories are shown in Table 1.

To verify the validity of our QCT results, the rate constant for the formation of  $\text{NH}_2\text{OH}^*$ , calculated from evaluated reactive cross sections and reaction probabilities, is compared with the available data in the literature. According to the collision theory, the reaction rate constant can be calculated as a function of reaction cross section  $\sigma(E)$  at temperature  $T$ .

$$k(T) = g_e \left( \frac{2}{K_B T} \right)^{3/2} (\pi\mu)^{-0.5} \int_0^\infty E \sigma(E) \exp(-E/K_B T) dE \quad (7)$$

where  $g_e$  is the ratio of electronic partition functions,  $g_e(T) =$

$\{4[1 + \exp(-201/T)]\}^{-1}$ ,  $\mu$  is the reactants reduced mass and  $K_B$  is the Boltzmann's constant.

As shown in Fig. 1, the formation of energized complex  $\text{NH}_2\text{OH}^*$ , reaction Rwa, is a barrier-less reaction. It has been noticed that a significant number of trajectories (around 6% to 20% depends on the relative kinetic energy) fall into the deep well of the potential energy surface, forming  $\text{NH}_2\text{OH}^*$ , and remain there on average up to  $2.3 \times 10^4$  steps at lower relative energies to  $1.6 \times 10^4$  steps at higher relative energies, thus leading to convergence problems. Table 2 summarizes the trajectory calculations, with non-converged trajectories removed from the total number of trajectories,  $N_T$ . The reactive encounters for the formation of energized intermediate  $\text{NH}_2\text{OH}^*$  were considered to calculate the average lifetime  $\langle \tau \rangle$  of  $\text{NH}_2\text{OH}^*$  [41,42]. The average lifetimes at  $25.2 \text{ kJ mol}^{-1}$  and  $157.5 \text{ kJ mol}^{-1}$  translational energy were calculated from lifetime distribution according to

$$\langle \tau \rangle = \sum_i \tau(N_i(\tau)/N_0)$$

where the summation is over 200 trajectories ( $N_0$ ) selected randomly from batches of 2000 trajectories. Each trajectory was terminated when the separation between the fragments of  $\text{NH}_2\text{OH}^*$  was  $4.5 \text{ \AA}$ . In measuring the lifetime, we have eliminated those encounters having lifetime less than 50 fs. The encounters for the formation of  $\text{NH}_2\text{OH}^*$  complex had a value of  $\langle \tau \rangle$  about 230 fs at  $25.2 \text{ kJ mol}^{-1}$  translational energy which decreased to a value of about 160 fs at  $157.5 \text{ kJ mol}^{-1}$  translational energy. The period of NO stretch in  $\text{NH}_2\text{OH}$  is about 35 fs. This value is much less than the calculated average lifetime. These average values of the lifetimes are valid in the absence of collisional deactivation. The collision frequency at 760 Torr is in the order of  $\sim 10^7 \text{ s}^{-1}$ .

As discussed in Ref. [41], at least, two IVR time scales are involved in association reactions like the formation of  $\text{NH}_2\text{OH}^*$  in this system. The first time scale is governed by the rate of IVR between relatively isolated O-N stretch mode and the reservoir of remaining modes when the energized intermediates are forming. The second time scale is the time needed for the required energy to find its way back into the reaction coordinates (N-O stretch mode) from the reservoir of other modes, to dissociate the newly formed

NH<sub>2</sub>OH\* intermediate. If the energy is not sufficient in the reaction coordinates for dissociation into the reactants or products, these intermediates must live long enough for energy to find its way back into the reaction coordinates. We do not intend to investigate the time scale for IVR or dissociation process and we have just reported the average life time of newly formed NH<sub>2</sub>OH\* intermediate.

In the absence of a potential energy barrier, the association reaction to form NH<sub>2</sub>OH\* complex should be controlled at low collisional energies by long-range interactions. The long range interactions are mainly associated to the permanent electric moments of the reactants. This indicates that formation of a complex is mainly dominated by the long-range potential and not by the internal dynamics of the complex. It is clear that the behavior of the H<sub>2</sub>N-OH bond potential from an intermediate to a long range has a major influence on the calculated recombination rate constants in the absence of the third body [43]. The reactive cross section,  $\sigma(E_{tr}) = \pi (b_{max})^2 P_r$ , may then be expressed by multiplying the capture cross section by a factor  $F_{rec}(E_{tr})$  that accounts for the recrossing effect.

$$\sigma(E) = AE_{tr}^\gamma F_{rec}(E_{tr}) \quad (8)$$

where  $A$  and  $\gamma$  are the fitting parameters. The recrossing ( $F_{rec}$ ) term depends on the translational energy and might be written as [43];

$$F_{rec}(E_{tr}) = \begin{cases} 1 & E_{tr} < E_{th} \\ \exp[-\alpha(E_{tr} + E_{th})] & E_{tr} \geq E_{th} \end{cases} \quad (9)$$

where  $E_{th}$  is regarded as threshold energy for recrossing process and  $\alpha$  is a fitting parameter. This expression denotes that once the energized intermediate NH<sub>2</sub>OH\* is formed, there is a probability for the recrossing process to take place. This recrossing process is proportional to certain effective value of the energy. This is given by the sum of the initial translational energy and an amount of energy depending on the internal energy of the reactants,  $E_{tr} + E_{th}$ , in the other words, the probability of a trajectory to recross back to the reactants after forming the energized NH<sub>2</sub>OH\* ( $P_{rec} = N_{rec}/N_C$ ) is increased when such effective energy is raised. Thus, the value of  $E_{th}$  is expected to be related to the initial energy content in the reactants.

Two parameters  $\alpha$  and  $E_{th}$  were found to be 0.06 and 0.51, respectively, by a non-linear least squares fitting of Eq. (9) to the data in Fig. 6,  $F_{rec} = (1 - P_{rec})$  vs.  $E_{tr}$ . As expected,  $E_{th}$  vanishes (or lies close to zero) in the

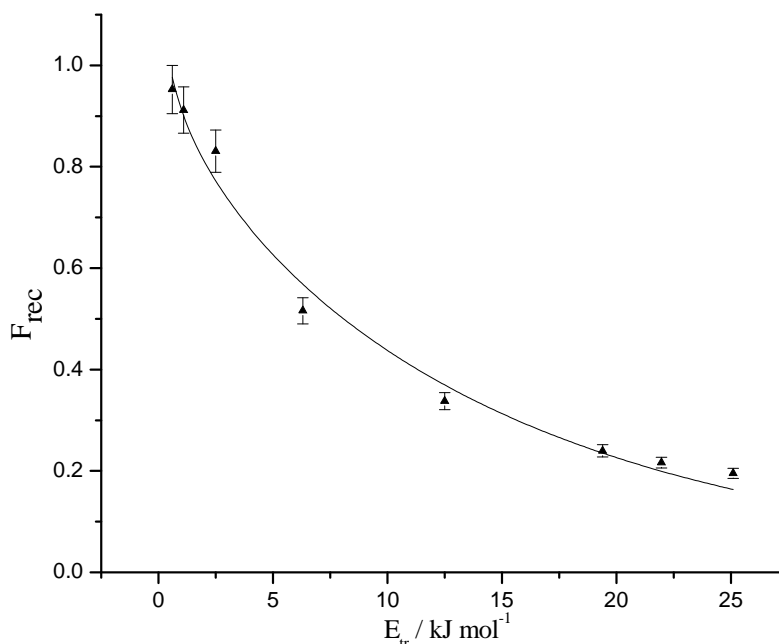


**Fig. 6.** Recrossing correction function as a function of relative translational energy.

traditional QCT method.

The calculated total reactive cross section is shown in Fig. 7, jointly with the results of the fitting based on Eq. (8). The total QCT reactive cross section shown in Fig. 7 for the MPWb1K surface could be approximately fitted to the following expression in unit of  $\text{Å}^2$ .

$$\sigma(E_{rr}) = 422.5E_{rr}^{-0.62} \exp(-0.06(E_{rr} + 0.51)) \quad (10)$$

After substitution of Eq. (8) into Eq. (7) and integration, one gets:

$$k(T) = k_{cap}(T) \times \exp(-\alpha E_{th}) \times \left( \frac{T_0}{T - T_0} \right)^{2+\gamma} \quad (11)$$

Where

$$k_{cap}(T) = A g_e(T) (K_B T)^{\gamma+1/2} \left( \frac{8}{\pi \mu} \right)^{1/2} \Gamma(\gamma+2) \quad (12)$$

where  $T_0 = 1/(\alpha K_B)$ , in which  $\Gamma(x)$  is the gamma function. By substituting Eq. (12) into Eq. (11), it is possible to express the rate constant, Eq. (7), as a function of temperature.

$$k(T) = 4.5 \times 10^{12} \times T^{-0.12} \times (0.50T + 1)^{-1.38} \quad 1 \text{ mol}^{-1} \text{ s}^{-1} \quad (13)$$

In Fig. 8 we have compared the calculated QCT rate constant for the formation of  $\text{NH}_2\text{OH}^*$  with the RRKM-SSA rate constant from Ref. [24] and experimental rate constant for the loss of the reactants from Ref. [5].

## CONCLUSIONS

QCT calculations carried out to study the behavior of energized  $\text{NH}_2\text{OH}^*$  formed by association collision of  $\text{NH}_2$  with OH. The QCT results reported here may be directly relevant to interstellar chemistry, where the pressure is low. It should be emphasized that quantum effects have been completely ignored here for the hydrogen transfer channels in this system. It is obvious that inclusion of quantum effect for hydrogen transfer channels increases the corresponding rate significantly, especially at lower temperatures, for instance rearrangement process of  $\text{NH}_2\text{OH}$  to  $\text{NH}_3\text{O}$ . According to QCT results, the branching ratio in Fig. 5

indicates that the formation of chemically activated  $\text{NH}_3\text{O}^*$  is not significant in this system.

As shown in Fig. 8, calculated QCT rate constant for the formation of  $\text{NH}_2\text{OH}^*$  is lower than the calculated rate constant from our previous study based on the RRKM-SSA method and the experimental values by Fagerstrom *et al.* reported for the loss of the reactants by a factor of 1.7 at lower temperature. In our QCT calculations no third body exists to remove the excess energy in newly formed energized  $\text{NH}_2\text{OH}^*$ . Therefore, the only possibility for stabilization of this chemically activated species is intramolecular vibrational redistribution (IVR). In Ref. [24], the RRKM-SSA formulation is based on the strong collision assumption for chemically activated species like  $\text{NH}_2\text{OH}^*$  that causes an upper limit rate constant for the stabilization process of the energized intermediates. Fagerstrom *et al.* did not measure the rate of formation of  $\text{NH}_2\text{OH}$ , instead they measured the decay rate of the reactants. The differential cross sections and reaction probability branching ratios of dissociative or rearrangement channels for the energized adducts are strongly affected by the initial relative translational energy of the reactants and their vibrational energy excitation.

The conservation of zero-point vibrational energy should also be maintained in classical trajectory studies of reaction dynamics. Figure 5 shows the product branching ratio, where only trajectories which lead to at least the (harmonic) zero-point vibrational energy in the products are counted. Probably the nonconservation of ZPE in some trajectories provides some indication of the uncertainties inherent in a classical trajectory estimate of branching ratios and normally causes an overestimation of the calculated probabilities.

In QCT calculations the lack of deactivation process causes the intramolecular vibrational redistribution (IVR) process be the only reason for the stabilization of highly vibrationally energized intermediates like  $\text{NH}_2\text{OH}^*$ . We found the branching ratio for the formation of  $\text{NH}_3\text{O}^*$  intermediate, in spite of our previous study, is very small, so we may assume the rearrangement process in  $\text{NH}_2\text{OH}^*$  for the formation of  $\text{CH}_3\text{O}^*$  could not occur easily or produced  $\text{CH}_3\text{O}^*$  dissociates easily because of the lack of third body collisions. This means that the vibrational energy in newly formed N-O bond in  $\text{NH}_2\text{OH}$  goes to one of N-H bonds to

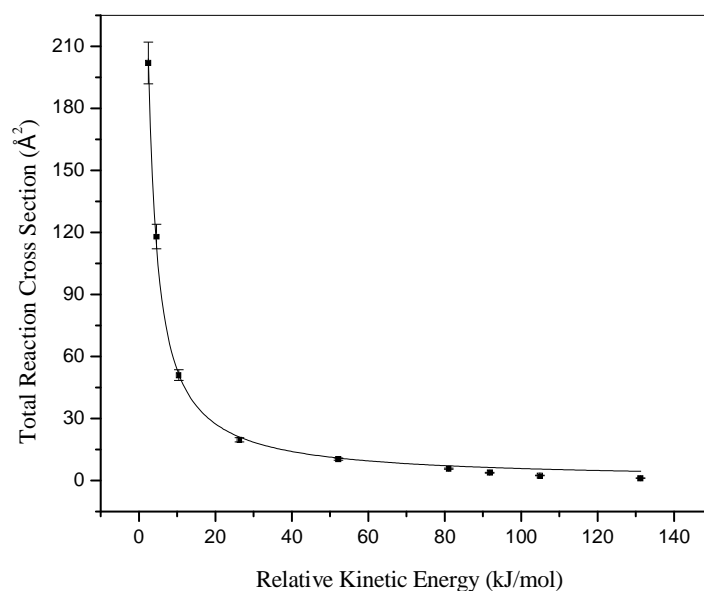


**Fig. 7.** Total reaction cross section as a function of relative kinetic energy for 2000 trajectories.

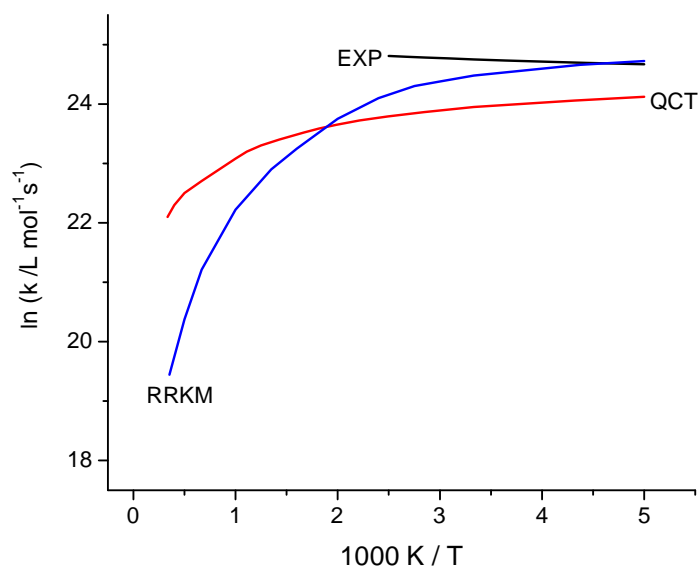


**Fig. 8.** Arrhenius plot for the formation of  $\text{NH}_2\text{OH}$ . (EXP) from Ref. [5], (RRKM) from Ref. [24], (QCT) present study.

form *cis* or *trans*-HNOH + H, the products of reactions R4 and R5, respectively, that causes the branching ratio for these products become more important, as shown in Fig. 5. The average lifetime distribution as a function of relative translational energy for the formation of  $\text{NH}_2\text{OH}^*$  is reported.

## ACKNOWLEDGEMENTS

The financial support of the Research Council of Shiraz University is acknowledged. Thanks to S. J. Hoseini for his mathematical helps.

## REFERENCES

- [1] J.A. Miller, C.T. Bowman, Prog. Energy. Combust. Sci. 15 (1989) 287.
- [2] A.M. Dean, J.E. Hardy, R.K. Lyon, 19<sup>th</sup> Symposium on International Combustion. The Combustion Institute, Pittsburgh, Pa. p. 97, 1982.
- [3] J.C. McConell, J. Geophys. Res. 78 (1973) 7812. Report of the NASA Working Group on Troposphere Program Planning: NASA Reference Publication; NASA: Washington, DC, p. 1062, 1980. Johnson, R. D., III. Computational Chemistry Comparison and Benchmark DataBase, <http://srdata.nist.gov/cccbdb/exp2.asp>. R.K. Lyon, Environ. Sci. Technol. 21 (1987) 231.
- [4] National Institute of Standard and Technology, <http://kinetics.nist.gov/kinetics>.
- [5] K. Fagerstrom, J.T. Jodkowski, A. Lund, E. Ratajczak, Chem. Phys. Lett. 236 (1995) 103.
- [6] K.H. Gericke, M. Loch, F. Schmidt, F. J.Comes, J. Chem. Phys. 101 (1994) 1988.
- [7] M.A. Kimball-Linne, R.K. Hanson, Combust. Flame, 64 (1986) 337.
- [8] N. Cohen, K.R. Westberg, J. Phys. Chem. Ref. Data, 20 (1991) 1211.
- [9] D.L. Baulch, C.J. Cobos, R.A. Cox, C. Esser, P. Frank, T. Just, J.A. Kerr, M.J. Pilling, J. Troe, R.W. Walker, J. Warnatz, J.J. Phys. Chem. Ref. Data 21 (1992) 411.
- [10] A.M. Dean, J.W. Bozzelli, in: W.C. Gardiner, Jr. (Ed.), Gas-Phase Combustion Chemistry, Springer-Verlag: New York, p. 125, 2000.
- [11] J.C. Mackie, G.B. Bacskay, J. Phys. Chem. A 109 (2005) 11967.
- [12] Z.-F. Xu, D.-C. Fang, X.-Y. Fu, Theor. Chem. Acc. 104 (2000) 7.
- [13] J. Shu, J.J. Lin, C.C. Wang, Y.T. Lee, X. Yang, J. Chem. Phys. 115 (2001) 842.
- [14] L. Wang, A.M. Mebel, X. Yang, X. Wang, J. Phys. Chem. A 108 (2004) 11644.
- [15] B.T. Hart, Aus. J. Chem. 29 (1976) 231.
- [16] S.S. Salimian, R.K. Hanson, C.H. Kruger, Combust. Flame 56 (1984) 83.
- [17] R.F. Hampson, Report No. FAA-EE-80-17; U.S. Dept. of Transport, 1980.
- [18] M.C. Branch, R.J. Kee, J.A. Miller, Combust. Sci. Technol. 29 (1982) 147.
- [19] K.J. Niemitz, H.G. Wagner, R.Z. Zellner, Phys. Chem. 124 (1981) 155.
- [20] E.C. Zebetta, P. Kilpinen, M. Hupta, K. Stahl, J. Leppalahti, M. Cannon, J. Nieminen, Energy Fuels 14 (2000) 751.
- [21] D.L. Baulch, D.D. Drysdale, D.G. Horne, A.C. Lloyd, Evaluated Kinetic Data for High Temperature Reactions, Butterworths: London 2 (1973) 483.
- [22] E.W.-G. Diau, T.-L. Tso, Y.-P. Lee, J. Phys. Chem. 94 (1990) 5261.
- [23] C.P. Fenimore, Combust. Flame 37 (1980) 245.
- [24] S.H. Mousavipour, F. Pirhadi, A.H. Agahi J. Phys. Chem. A 113 (2009) 12961.
- [25] J.L. Scott, D. Luckhaus, S.S. Brown, F.F. Crim, J. Chem. Phys. 102 (1995) 675.
- [26] J.N. Murrell, S. Carter, S. Frantos, P. Huxley, A.J.C. Varandas, Molecular Potential Energy Functions Wiley, New York, p. 206, 1984.
- [27] K.B. Lipkowitz, D.B. Boyd, Review in Computational Chemistry VCH, New York, 1990.
- [28] R. Car, M. Parrinello, Phys. Rev. Lett. 55 (1985) 2471.
- [29] P.A. Ryan, J. Bettens, Am. Chem. Soc. 125 (2003) 584.
- [30] Ischtwan, M.A. Collins, J. Chem. Phys. 100 (1994) 8080. K.C. Thompson, M.J.T. Jordan, M.A. Collins, J. Chem. Phys. 102 (1995) 5647. M.J.T. Jordan, K.C. Thompson, M. A. Collins, J. Chem. Phys. 108 (1998) 8302. R.P.A. Bettens, M.A. Collins, J. Chem. Phys. 111 (1999) 816. R.P.A. Bettens, M.A. Collins, J. Chem. Phys. 108 (1998) 2424.
- [31] R.O. Fuller, R.P.A. Bettens, M.A. Collins, J. Chem. Phys. 114 (2001) 10711. M.A. Collins, S. Petrie, A.J. Chalk, L. Radom, J. Chem. Phys. 112 (2000) 6625. R.P.A. Bettens, T.A. Hansen, M.A. Collins, J. Chem. Phys. 111 (1999) 6322. M.A. Collins, R.P.A. Bettens, Phys. Chem. Chem. Phys. 1 (1999) 939. R.P.A. Bettens, M.A. Collins, J. Chem. Phys. 109 (1998) 9728R. P.A. Bettens, M.A. Collins, J. Chem. Phys. 108 (1998) 2424. D.H. Zhang, M.A. Collins, S.-Y. Lee, Science 290 (2000) 961. R.P.A. Bettens, M.A.

- Collins, M.J.T. Jordan, D.H. Zhang, *J. Chem. Phys.* 112 (2000) 10162.
- [32] K.C. Thompson, M.A. Collins, *J. Chem. Soc., Faraday Trans.* 93 (1997) 871.
- [33] K.C. Thompson, M.J.T. Jordan, M.A. Collins, *J. Chem. Phys.* 108, Ryan P.A. Bettens and Michael A. Collins, *J. Chem. Phys.* 111 (1999) 8302.
- [34] R. Farwig, in: J.C. Mason, M.G. Cox (Eds.), *Algorithms for Approximation*, Clarendon, Oxford, 1987, p. 194. 16P. Lancaster and K. Salkauskas, *Curve and Surface Fitting, An Introduction*, Academic, London, 1986.
- [35] M.W. Schmidt, K.K. Baldrige, J.A. Boatz *et al.*, *J. Comput. Chem.* 14 (1993) 1347.
- [36] J.R.P.A. Bettens, M.A. Collins, *J. Chem. Phys.* 111 (1999) 15.
- [37] H.M. Netzloff, M.A. Collins, M.S. Gordon *J. Chem. Phys.* 124 (2006) 154104.
- [38] M.J.T. Jordan, K.C. Thompson, M.A. Collins, *J. Chem. Phys.* 102 (1995) 5647.
- [39] A. Varandas, *J. Chem. Phys.* 99 (1993) 1076.
- [40] A. Varandas, *Chem. Phys. Lett.* 225 (1994) 18.
- [41] L.M. Yoder, J.R. Barker, *J. Phys. Chem. A* 104 (2000) 10184.
- [42] Y. Liu, L.L. Lohr, J.R. Barker, *J. Phys. Chem. A* 110 (2006) 1267. Y. Liu, L.L. Lohr, J.R. Barker, *J. Phys. Chem. B* 109 (2005) 8304.
- [43] M.Y. Ballester, A.J.C. Varandas, *Chem. Phys. Lett.* 433 (2007) 279.